

4

AD-A211 586

OFFICE OF NAVAL RESEARCH

Contract N00014-87-K-0494

R&T Code 400X027YIP

Technical Report No. 6

Effect of Electrical Double Layer on Transport Limited Currents at Microelectrodes

by

J. D. Norton, H. S. White, and S. W. Feldberg

Prepared for Publication in the

Journal of Physical Chemistry

University of Minnesota
Department of Chemical Engineering and Materials Science
Minneapolis, MN 55455

July, 1989

Reproduction in whole or in part is permitted for any purpose of the United States Government.

This document has been approved for public release and sale; its distribution is unlimited.

014
a

88 014

REPORT DOCUMENTATION PAGE

| | | | |
|---|--|---|-------------------------|
| 1a. REPORT SECURITY CLASSIFICATION Unclassified | | 1b. RESTRICTIVE MARKINGS | |
| 2a. SECURITY CLASSIFICATION AUTHORITY | | 3. DISTRIBUTION AVAILABILITY OF REPORT Unclassified/Unlimited | |
| 2b. DECLASSIFICATION/DOWNGRADING SCHEDULE | | | |
| 4. PERFORMING ORGANIZATION REPORT NUMBER(S) ONR Technical Report 6 | | 5. MONITORING ORGANIZATION REPORT NUMBER(S) | |
| 5a. NAME OF PERFORMING ORGANIZATION Dept of Chemical Engineering and Materials Science | 5b. OFFICE SYMBOL (if applicable) Code 1113 | 7a. NAME OF MONITORING ORGANIZATION Office of Naval Research | |
| 5c. ADDRESS (City, State, and ZIP Code) University of Minnesota Minneapolis, MN 55455 | | 7b. ADDRESS (City, State, and ZIP Code) 800 North Quincy Street Arlington, VA 22217 | |
| 8a. NAME OF FUNDING/SPONSORING ORGANIZATION Office of Naval Research | 8b. OFFICE SYMBOL (if applicable) | 9. PROCUREMENT INSTRUMENT IDENTIFICATION NUMBER Contract No. N00014-87-K-0494 | |
| 8c. ADDRESS (City, State, and ZIP Code) 800 North Quincy Street Arlington, VA 22217-5000 | | 10. SOURCE OF FUNDING NUMBERS | |
| | | PROGRAM ELEMENT NO. | PROJECT NO. |
| | | TASK NO. | WORK UNIT ACCESSION NO. |
| 11. TITLE (Include Security Classification) Effect of the Electrical Double Layer on Transport Limited Currents at Microelectrodes | | | |
| 12. PERSONAL AUTHOR(S) John D. Norton and Henry S. White and S.W. Feldberg | | | |
| 13a. TYPE OF REPORT Technical | 13b. TIME COVERED FROM _____ TO _____ | 14. DATE OF REPORT (Year, Month, Day) | 15. PAGE COUNT |
| 16. SUPPLEMENTARY NOTATION prepared for publication in the Journal of Physical Chemistry | | | |
| 17. COSATI CODES | | 18. SUBJECT TERMS (Continue on reverse if necessary and identify by block number) | |
| FIELD | GROUP | SUB-GROUP | |
| | | | |
| | | | |
| 19. ABSTRACT (Continue on reverse if necessary and identify by block number) <p>An analysis of transport of charged and uncharged species associated with a steady-state faradaic process at a spherical microelectrode is reported. We examine systems comprising various relative concentrations of a redox species, and, if charged, its counter ion, and an inert electrolyte. Of particular interest is the behavior of these systems when the thickness of the diffuse double layer (characterized by the Debye length, κ^{-1}) and the radius of the electrode (r_0) are comparable. Transport of each species is assumed to be governed by the Nernst-Planck equation. A generalized solution obtained using finite-difference simulations demonstrates that significant enhancement or inhibition of the steady-state flux can occur and will depend upon the dimensionless parameter $r_0\kappa$, upon the relationship between the applied potential (E_{app}), the formal redox potential (E^0), and the potential of zero charge (E_{pzc}), and upon the charges and relative concentrations of the species in solution. Analytic solutions for several limiting cases are discussed and serve as simple expositions of the phenomena as well as a verification of the simulations. (continued on next page)</p> | | | |
| 20. DISTRIBUTION AVAILABILITY OF ABSTRACT <input checked="" type="checkbox"/> UNCLASSIFIED/UNLIMITED <input type="checkbox"/> SAME AS RPT <input type="checkbox"/> DTIC USERS | | 21. ABSTRACT SECURITY CLASSIFICATION Unclassified | |
| 22a. NAME OF RESPONSIBLE INDIVIDUAL Henry S. White | | 22b. TELEPHONE (Include Area Code) (612) 625-6995 | 22c. OFFICE SYMBOL |

Effect of the Electrical Double Layer on Transport Limited Currents at Microelectrodes

John D. Norton and Henry S. White
Department of Chemical Engineering and Materials Science
University of Minnesota
Minneapolis, MN 55455

and

Stephen W. Feldberg
Brookhaven National Laboratory
Upton, NY 11973

Abstract. An analysis of transport of charged and uncharged species associated with a steady-state faradaic process at a spherical microelectrode is reported. We examine systems comprising various relative concentrations of a redox species and, if charged, its counter ion, and an inert electrolyte. Of particular interest is the behavior of these systems when the thickness of the diffuse double layer (characterized by the Debye length, κ^{-1}) and the radius of the electrode (r_0) are comparable. Transport of each species is assumed to be governed by the Nernst-Planck equation. A generalized solution obtained using finite-difference simulations demonstrates that significant enhancement or inhibition of the steady-state flux can occur and will depend upon the dimensionless parameter $r_0\kappa$, upon the relationship between the applied potential (E_{app}), the formal redox potential (E^0), and the potential of zero charge (E_{pzc}), and upon the charges and relative concentrations of the species in solution. Analytic solutions for several limiting cases are discussed and serve as simple expositions of the phenomena as well as a verification of the simulations. In infinitely dilute ionic solutions, i.e., $r_0\kappa \rightarrow 0$, the limiting flux of ionic species may be computed directly from the Smoluchowski-Debye theory for ionic bimolecular reaction rates. Computation of theoretical voltammograms in the limit of infinite dilution (i.e., $r_0\kappa \rightarrow 0$) reveals the surprising result that under certain reaction conditions the steady-state current-voltage curve will be peaked rather than sigmoidal giving the appearance that electrochemical activity occurs only within a small (several hundred millivolt) potential window. The effect is easily explained when the electric field, and the charge of the reacting species is considered. Implications in the design of microscopic redox substrates, e.g., dispersed metal catalysts, are discussed.

Introduction. Development of electrochemical applications of microelectrodes has flourished during the last decade expanding considerably beyond early applications as biological stimulators and sensors^{1,2}. The development has been driven by advances in solid state technology which continues to produce faster and more sensitive electronic devices as well as novel techniques for the fabrication of microelectrode devices . It is now possible to produce a microelectrode or microelectrode array whose critical dimension, r_0 (e.g., the half-width of a band electrode or the radius of its hemicylindrical approximation; the radius of a disk electrode or its hemispherical approximation), is of the order of tens of angstroms^{3,4}. The reduced iR error associated with a microelectrode coupled with increasingly fast and sensitive amplifiers permits extremely fast voltage perturbations and current measurement, e.g., cyclic voltammetry at $\sim 2 \times 10^6$ V/s, thereby accessing a new time domain in electrochemical measurements. The size of an electrode dictates the spatial (as well as the time) domain that is probed and an electrode with angstrom dimensions may reveal fundamental information about the solvent structure and ion distribution within a few angstroms of the electrode surface.

When a microelectrode having an r_0 as small as 10^{-7} cm, ^{3,4} operates in an electrolyte concentration in the range of 10^{-5} - 10^{-1} M, the thickness of the diffuse double layer (characterized by the Debye length, κ^{-1}) is comparable with or much larger than the diffusion layer δ . It is thus meaningful (and necessary) to ask how the overlap of the diffusion layer and diffuse double layer will affect the fluxes and spatial distributions of the various solution species. For example, consider a spherical electrode of radius r_0 in contact with a solution containing a redox active ion (e.g., A^+) as well as supporting electrolyte, Fig. 1. The characteristic lengths κ^{-1} and δ have different dependencies on the electrode radius, r_0 , and the chemical composition of the electrolyte. In a solution containing a symmetrical electrolyte, κ^{-1} is proportional to the inverse square root of the

total ionic concentration, $C^{-1/2}$, and independent of the electrode radius, r_0 . Conversely, δ is proportional to r_0 and independent of C . The relative thicknesses of the diffuse double layer and the depletion layer determine the extent to which ion transport is affected by the former. At macroscopic electrodes, $\kappa^{-1} \ll \delta$, the double layer has an insignificant effect on the rate at which ions are transported to the surface. However, κ^{-1} can become comparable to δ by either decreasing the ionic concentration or the electrode radius. When $\kappa^{-1} \geq \delta$, the transport and net current of reactant ions will be increased or decreased by the electric field originating at the electrode surface.

We are particularly interested in the behavior (at microelectrodes) of systems comprising a redox species and its counter ion with little or no supporting electrolyte. The generalized system comprises 4 chemical species: a redox couple, O^{z_O} , R^{z_R} related by



along with a pair of supporting electrolyte components, X^{z_X} and Y^{z_Y} . The systems we examine may initially contain as few as two species (e.g., O^{z_O} and X^{z_X}) with the faradaic process producing R^{z_R} (eq. 1). The generalized problem is solved by presuming that transport and distribution of all species is governed by the Nernst-Planck equation and by classical electrostatics. The resulting set of equations are solved using a finite difference methodology. In order to simplify our inquiry we consider only spherical geometry. This not only simplifies the computations, but also permits us to discuss true steady-state fluxes. However, the results are qualitatively applicable to any geometry and comparable r_0 .

A number of workers have considered migration effects at microelectrodes. With presumption of spherical geometry and the constraint of electroneutrality (corresponding to the limiting case where $r_0\kappa \rightarrow \infty$, i.e., $\kappa^{-1} \ll r_0$) they can obtain some useful analytic expressions for the steady-state flux. Bond et al, also mention (but do not calculate) the

infinite dilution limit (the "single-ion case") which occurs when $r_0\kappa \rightarrow 0$ (i.e., $\kappa^{-1} \gg r_0$). Electrostatic ion-ion interaction is negligibly small compared to the interaction with the electric field produced by the charge on the electrode. We shall present the analytic solution for that limiting case since it provides a simple basis for understanding the more complicated systems. We shall also discuss several other limiting cases which have analytic solutions (the aforementioned electroneutrality limit, the trivial diffusion limit attained with an excess of supporting electrolyte, and the zero-current equilibrium (spherical) diffuse double layer^x). The simulations serve to identify the range of $r_0\kappa$ values appropriate for analytic solutions.

Results and Discussion.

At sufficiently low concentrations of supporting electrolyte or small electrode radii, $r_0\kappa \rightarrow 0$, the number of ions surrounding the electrode is negligible, resulting in an unscreened electrostatic force between the electrode and redox ions. Analysis of this limiting case is developed in three main sections. First, we derive an exact solution for current-voltage behavior as $r_0\kappa \rightarrow 0$. We then report finite-difference simulations of the flux as a function of $r_0\kappa$ and concentration to determine the useful working range of the analytic solution. In the final section, we present examples of steady-state voltammograms expected as $r_0\kappa \rightarrow 0$.

General current-voltage relationship as $r_0\kappa \rightarrow 0$

The i - V expression is obtained for the situation in which the solution contains both reduced and oxidized forms of a redox couple ($O^{z_O} + (z_O - z_R)e^- \rightarrow R^{z_R}$). For clarity, the superscripts z_O and z_R are omitted.

Assuming that the electron-transfer reaction is governed by Butler-Volmer kinetics, the net flux to the electrode surface is given by

$$\frac{i}{nFA} = k_0 [C_O^s \exp^{-\alpha n f \eta} - C_R^s \exp^{(1-\alpha) n f \eta}] \quad (2)$$

where k_0 is the standard heterogeneous rate constant, α is the transfer coefficient, $f = F/RT$, and $\eta = (E - E^0)$. The surface concentrations C_O^s and C_R^s in the limit $r_0 \kappa \rightarrow 0$ can be obtained by solving for the diffusional-migrational fluxes of O and R. We assume that the flux of all species is governed by the Nernst-Planck equation

$$f_j = -D_j \frac{dC_j}{dr} + D_j \frac{F}{RT} \mathcal{E} C_j z_j \quad (3)$$

For an unscreened spherical electrode, the electric field resulting from the charged electrode is defined by:

$$\mathcal{E} = \mathcal{E}_{r=r_0} \left(\frac{r_0}{r} \right)^2 \quad (4)$$

Substitution of eq. 4 into the Nernst-Planck equation (eq. 2) yields

$$f_j = -D_j \frac{dC_j}{dr} + D_j C_j W_j / r^2 \quad (5)$$

where $W_j = (F/RT) z_j r_0 \mathcal{E}_{r=r_0}$. The dimensionless group W_j can be rewritten in terms of experimentally defined parameters by substituting the expression

$$\mathcal{E}_{r=r_0} = - \left(\frac{d\phi}{dr} \right)_{r=r_0} = (4\pi\epsilon\epsilon_0 r_0^2)^{-1} \sigma, \quad (6)$$

to yield
$$W_j = \frac{\phi_0 z_j e^-}{kT} \quad (7)$$

In this form, W_j is recognized as the dimensionless unscreened electrostatic interaction energy between the electrode at potential ϕ_0 and the ion of charge z_j .

The equation of continuity, for a spherical coordinate system applied to species j yields

$$\frac{d}{dr}(r^2(-D_j \frac{dC_j}{dr} + D_j C_j W_j / r^2)) = 0 \quad (8)$$

which can be integrated and evaluated using the boundary conditions

$$C_j = C_j^* \quad \text{as } r \rightarrow \infty \quad (9)$$

$$C_j = C_j^s \quad \text{at } r = r_0$$

to yield the concentration profile of j , eq. 10.

$$C_j = C_j^* \left[\frac{(C_j^s / C_j^* - 1)(e^{-W_j r_0 / r} - 1)}{e^{-W_j} - 1} \right] + 1 \quad (10)$$

Substitution of eq. 10 into eq. 5. yields the flux of species j evaluated at the electrode surface, $r = r_0$.

$$f_j = \frac{W_j D_j C_j^*}{r_0} \left[\frac{e^{-W_j} - C_j^s / C_j^*}{e^{-W_j} - 1} \right] \quad (11)$$

Rearranging eq. 10 to obtain the surface concentrations of O and R yields

$$C_{O^s} = C_{O^*} \left[e^{-W_O} - \frac{r_0(f_O)(e^{-W_O} - 1)}{D_O C_{O^*} W_O} \right] \quad (12)$$

and

$$C_{R^s} = C_{R^*} \left[e^{-W_R} - \frac{r_O(f_R)(e^{-W_R} - 1)}{D_R C_{R^*} W_R} \right] \quad (13)$$

From the stoichiometry of eq. 1, $f_O = -f_R$. In addition, $\frac{i}{nFA} = -f_O$ (the sign convention used in writing eq. 2 indicates that the reduction of O results in a positive current; because a positive species flux corresponds to transport away from the surface, a negative flux of O corresponds to a positive current). Using these relationships and substituting eqs. 12 and 13 into the Butler-Volmer equation (eq. 2) yields the general i-E relationship in the limit $r_O \kappa \rightarrow 0$,

$$\frac{i}{nFA} = \frac{e^{-W_O} C_O^* k_f - e^{-W_R} C_{R^*} k_r}{1 - \frac{r_O}{D} \left[\frac{(e^{-W_O} - 1) k_f}{W_O} + \frac{(e^{-W_R} - 1) k_r}{W_R} \right]} \quad (14)$$

where $k_f = k_0 e^{-\alpha n f \eta}$ and $k_r = k_0 e^{(1-\alpha) n f \eta}$. Several limiting cases of this general flux equation are considered below.

I. $W \rightarrow 0$

This limit corresponds to purely diffusional controlled transport of both O or R, which is difficult to obtain in the strictest sense since both the electrode and either O or R has a net charge. However, for a macroscopic electrode in a concentrated electrolyte solution, the electric field originating from the electrode rapidly decays to a small value at a very short distance compared to the diffusion layer thickness, δ . Under these conditions, the charge on the electrode is fully screened and the effective interaction energy, W_j , at distances greater than $\sim 2\kappa^{-1}$ is zero. The dominant transport resistance is diffusion of O

and R through the depletion layer, unaffected by the electric field in the thin double layer.

In this limit, eq. 14 reduces to

$$\frac{i}{nFA} = \frac{(C_O^*k_f - C_R^*k_r)}{1 + \frac{r_0}{D}(k_f + k_r)} \quad (15)$$

which is identical to the result obtained by Shain et. al. for spherical electrodes⁵. The criteria for a reversible electron-transfer reaction is $\frac{k_0}{k_{m.t.}} \gg 1$, where the mass-transport

rate is defined as $k_{m.t.} = D/r_0$. When this criteria is satisfied, eq. 15 yields

$$E = E^{o'} + \frac{RT}{nF} \ln \frac{(i_L^c(diff.) - i)}{(i - i_L^a(diff.))} \quad (16a)$$

where $i_L^c(diff.) = nFADC_O^*/r_0$ and $i_L^a(diff.) = -nFADC_R^*/r_0$.

II. $W_j \neq 0$ and Reversible Electron-Transfer.

The criteria of a reversible electron-transfer reaction remains $\frac{k_0}{k_{m.t.}} \gg 1$. However, the mass-transport rate is now given by $k_{m.t.} = \frac{DW_j}{r_0(1 - e^{-W_j})}$, which is a potential dependent

quantity. When $k_0 \gg k_{m.t.}$, eq. 14 reduces to eq. 16b

$$E = E^{o'} + \frac{RT}{nF} \ln \frac{(i_L^c - i)}{(i - i_L^a)} \quad (16b)$$

where the migration-diffusion limited currents are given by

$$i_L^c = -\frac{nFADC_O^*}{r_0} \left[\frac{W_O}{1 - e^{-W_O}} \right] \quad (17)$$

and

$$i_L^a = \frac{nFADC_R^*}{r_0} \left[\frac{W_R}{1 - e^{-W_R}} \right] \quad (18)$$

It is noteworthy that $k_{m.t.}$ is dependent on the electrostatic potential $\phi_0 (= E - E_{pzc})$ for all E , a result of electrostatic attraction or repulsion of the reactant. This is in contrast to a purely diffusional controlled rate which is independent of E at sufficiently large values of η . A consequence of the dependence of $k_{m.t.}$ on ϕ_0 is that the apparent reversibility of the electron-transfer reaction will depend on the relative values of $E^{o'}$ and E_{pzc} . In addition, eqs. 17) and 18 indicate that no steady-state limiting current plateau is expected when W_j is finite. We return to these points when we consider specific examples of the voltammetric behavior of a spherical microelectrode in the limit $r_0\kappa \rightarrow 0$.

III. Normalized Limiting Flux at Large η and Finite W_j

Dividing eqs. 17 and 18 by the corresponding limiting diffusional fluxes in the absence of migration (i.e., $W_j \rightarrow 0$), $i_{L^c}(\text{diff.}) = nFADC_O/r_0$ (for reduction) and $i_{L^a}(\text{diff.}) = -nFADC_R/r_0$ (for oxidation), yields the normalized limiting current to a spherical electrode in the limit $r_0\kappa \rightarrow 0$

$$\frac{i_L}{i_{L(\text{diff.})}} = \frac{W_j}{e^{W_j} - 1} \quad (19)$$

Eq. 19 indicates that the normalized flux is dependent only on the electrode potential (vs. E_{pzc}) and the charge of the reactant z_j . The normalized flux is independent of the electrode radius as $r_0\kappa \rightarrow 0$, a point we shall return to later in discussing finite difference simulations of the flux.

An alternative and more intuitive approach in analyzing the transport limited flux (large η) at microelectrodes is to treat the electrode as a small stationary sphere (i.e., an ion) that reacts with freely diffusing reactant in a bimolecular collision. The rate of such a reaction between ions in an infinitely dilute solution was originally considered by Debye⁶ using Smoluchowski's method⁷ and shown to be dependent on the charges of the two reactants. If the diffusivity of one of the ions is set equal to zero (corresponding to the

stationary electrode) and the radius of the other set to zero (corresponding to a point charge reactant), the Smoluchowski-Debye equation yields eq. 19, the flux to a spherical microelectrode (see Appendix). The enhancement or inhibition of bimolecular rates predicted by Debye results from the electrostatic force between the reactant ions. In general, because the valencies of ions in solution are relatively low (+4 to -4), bimolecular transport controlled rate constants in aqueous solutions do not vary by more than a factor of 3 or 4 from the diffusional controlled rate constant for uncharged species. The effective valence, z_{elec} , of a spherical microelectrode is given by eq. 20.

$$z_{elec} = 4\pi\epsilon\epsilon_0(E-E_{pzc})r_0/e^- \quad (20)$$

In comparison to the charge of a solution ion, z_{elec} , can be potentiostatically controlled and set to exceeding large values. For example, at 0.1 V vs E_{pzc} , z_{elec} for a 100Å electrode is +54 and the normalized flux (relative to an uncharged species) for the oxidation of a monovalent cation is 0.081. Under the same conditions, if the electrode potential is poised at 0.5 V vs E_{pzc} , the z_{elec} increases to +270 and the normalized flux decreases to a negligible value, 6.8×10^{-8} . Conversely, an enhancement of the normalized flux is predicted for the reduction of a monovalent cation at electrode potentials more negative than E_{pzc} .

Finite-Difference Simulation. In this section, we report finite difference simulation of the transport limited flux at large η for two specific electrochemical reactions. The results obtained allow a useful estimate of the maximum permissible value of $r_0\kappa$ for applying the analytic solution presented above. The simulations also yield the flux for intermediate values of $r_0\kappa$. The model utilizes the finite-difference method to simulate the current and ion distribution occurring at a spherical microelectrode of radius, r_0 . The electrochemical

reactions considered are the 1-e⁻ reduction of a singly charged cation ($A^+ + e^- \rightarrow A$) and the 1-e⁻ oxidation of singly charged anion ($A^- \rightarrow A + e^-$). The solution contains reactant (A^+ or A^-) and a 1:1 electrolyte which shares a common counterion. The spherical working electrode is assumed to be surrounded by a large concentric spherical counterelectrode, maintaining a radial flux under all conditions.

The finite-difference program calculates the time-dependent fluxes and concentrations of all species following a potential step to the electrode at $t = 0$. Initially, the electrode is assumed to be uncharged with respect to the solution, and all species are distributed uniformly throughout the solution. At $t = 0$, a potential (ϕ_0) of +0.1V versus E_{pzc} is applied to the electrode. The potential step is assumed to be sufficiently large to cause the mass-transfer limited reduction (or oxidation) of A^+ (or A^-) at the limiting current plateau. Only the final steady-state fluxes are reported here.

The model considers migration resulting from electric fields established by the diffusive ion flux as well as that due to the charged electrode surface. At any point in solution a distance r from the electrode surface, the flux of species j in the radial direction is given by the Nernst-Planck equation (eq 3). The time-dependent net flux of charged species gives rise to a time-dependent electric field which is represented by:

$$\frac{d\mathcal{E}}{dt} = - \frac{F \sum f_j z_j}{\epsilon \epsilon_0} \quad (21)$$

The digital simulation is based on a system devised by Joslin and Pletcher⁸ and modified by Feldberg⁹, employing the finite-difference method with an exponential space grid and modified to incorporate the DuFort Frankel algorithm¹⁰. A detailed description of the simulations will be presented in a forthcoming publication¹¹.

A preliminary test of the accuracy of the model and the numerical calculations was made by simulating the equilibrium concentration profiles of a 1:1 electrolyte within the

diffuse double layer for the case in which no faradaic reaction occurs. These results were compared to numerical values tabulated by Loeb, et. al.,¹² using Gouy-Chapman theory, for spherical colloidal particles.

Fig. 2a-c shows a comparison of the ion concentration profiles generated by digital simulation (solid lines) with the results of Loeb, et. al.(points), for 5, 50, and 100 Å radius spherical electrodes. The bulk concentration of the 1:1 electrolyte (0.148 - 372 mM) and the surface potential (0.026 - 0.103 V) used in the simulations are indicated in each figure. In all cases, excellent agreement (within 1 %) is obtained between the simulated profile and the numerical results of Loeb, et. al.

Simulated Fluxes.

Transport limited steady-state currents obtained from finite-difference simulations corresponding to the 1-e⁻ reduction of a +1 species ($A^+ + e^- \rightarrow A$) and the 1-e⁻ oxidation of a -1 species ($A^- \rightarrow A + e^-$) are shown in Fig. 3. In each system, we assume an 1:1 supporting electrolyte, an applied potential of +0.1 V versus E_{pzc} , and zero product concentration in the bulk. The results are plotted in Fig. 3 as a function of $r_0\kappa$ (corresponding to electrode radii ranging from 5 to 10,000 Å, and supporting electrolyte concentrations from 10^{-7} to 10 M). Each line in Fig. 3 corresponds to a different ratio of the concentrations of reactant (A^+ or A^-) to supporting electrolyte, C_{redox}/C_{elec} .

Numerical values of limiting currents have been normalized to the current expected at a sphere for a purely diffusion controlled reaction ($i_L(diff.) = 4\pi nFD C^* r_0$ where C^* is the bulk reactant concentration). Thus, the horizontal line at $i/i_L(diff.) = 1$ in Fig. 3 corresponds to the oxidation or reduction of a neutral reactant.

Fig. 3 shows that a deviation from classical diffusion limited current is observed as $r_0\kappa$ decreases or as C_{redox}/C_{elec} increases. This behavior results from two distinctly

different phenomena: (i) migration resulting from depletion of reactant ions at the electrode and (ii) migration resulting from the electrostatic field originating at the surface.

(i) *Migration resulting from depletion of reactant ions at the electrode.*

At large $r_0\kappa$ (e.g., corresponding to a macroscopic electrode), the current for either the reduction of A^+ or the oxidation of A^- to the neutral A increases to a value approximately twice as large as the purely diffusional current when the electrolyte concentration becomes appreciably smaller than the reactant concentration, $C_{\text{redox}}/C_{\text{elec}} > 10^2$ (Fig. 3). This behavior was first described quantitatively by Heyrovsky¹³ and Ilkovic¹⁴ and more recently addressed in context of microelectrode behavior in solutions of low ionic strength^{xxxx}. In the limit of little or no supporting electrolyte, the system can be approximated as containing three species in solution, the charged reactant, $j=1$, its corresponding counterion, $j=2$, and the neutral product, $j=3$. Solution electroneutrality requires that:

$$C_1 z_1 + C_2 z_2 = 0 \quad (22)$$

and:
$$\frac{dC_1}{dr} z_1 + \frac{dC_2}{dr} z_2 = 0 \quad (23)$$

Using eq. 3 to define the fluxes of reactant and counterion:

$$f_1 = -D_1 \frac{dC_1}{dr} + D_1 \frac{F}{RT} \epsilon C_1 z_1 \quad (24)$$

$$f_2 = 0 = -D_2 \frac{dC_2}{dr} + D_2 \frac{F}{RT} \epsilon C_2 z_2 \quad (25)$$

and substituting eqs. 22, 23, 25 into eq.24 yields the steady-state reactant flux:

$$f_1 = -D_1 \frac{dC_1}{dr} \left(1 - \frac{z_1}{z_2}\right) \quad (26)$$

Combining eq.26 with the continuity equation for a spherical system ($\frac{d}{dr} (r^2 f_j) = 0$), and integrating using the boundary conditions $C \rightarrow C^b$ as $r \rightarrow \infty$ and $C = 0$ at $r=r_0$ yields the expected transport limited current:

$$i_L = 4\pi n F D C^b r_0 \left(1 - \frac{z_1}{z_2}\right) \quad (27)$$

In solutions containing a monovalent reactant (A^+ or A^-) and a monovalent counterion of opposite charge (X^- or X^+), the limiting current (eq. 27) for cation reduction or anion oxidation should increase by a factor of 2 relative to the diffusion limited current in the presence of excess supporting electrolyte, $i_L(\text{diff.})$.

The dotted line in Fig. 3 shows the asymptotic limiting value of 2 that the normalized current approaches as $C_{\text{redox}}/C_{\text{elec}}$ increases. We find that that $i_L/i_L(\text{diff.})$ for the oxidation of A^- equals 2 for $C_{\text{redox}}/C_{\text{elec}} \gg 10^3$. However, for the same values of $C_{\text{redox}}/C_{\text{elec}}$ and $r_0\kappa$, $i_L/i_L(\text{diff.})$ is significantly smaller for the reduction of A^+ , ~ 1.32 , than the expected value of 2. We show in the following section that this deviation is due to electrostatic repulsion between the positively charged electrode ($\phi_0 = 0.1$ V) and A^+ .

(ii) *Migration resulting from the electrostatic field originating at the electrode surface.*

For $r_0\kappa < 50$, the limiting current deviates from the diffusional currents even when the supporting electrolyte concentration is considerable larger than the redox active concentration. For example, the current corresponding to the oxidation A^- at $r_0\kappa = 10$ $C_{\text{redox}}/C_{\text{elec}} = 10^{-2}$ is $\sim 20\%$ larger than the purely diffusional controlled value. The reduction of A^+ yields a current that is 55% smaller than the purely diffusional controlled

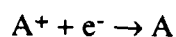
value. We ascribe these deviations from a purely diffusional response to electrostatic double layer forces acting on the reactant within the depletion layer. Qualitatively, the flux of an anionic reactant, to a positively charged electrode is expected to be increased, resulting from electrostatic attraction. Conversely, the flux of cationic reactant would be decreased. This behavior is observed in Fig. 3 for the reaction of +1 and -1 species at a positively charged electrode ($\phi_0 = 0.1$ V).

As anticipated, the effect of the electrical double layer on migrational currents becomes more pronounced as $r_0\kappa$ decreases. This behavior reflects the relative dimensions of the double layer with respect to the depletion length, which in turn is determined by the electrode radius and electrolyte concentration (see Fig. 1). For $\kappa^{-1} \ll r_0$ (i.e., large $r_0\kappa$), the thickness of the double layer is insignificant compared to the depletion length ($\sim 10r_0$), and reactant ions do not experience an electrostatic force until they are in the immediate vicinity of the electrode. Under these circumstances, ions diffuse to the surface across an *electroneutral depletion layer*. Conversely, for $\kappa^{-1} \geq r_0$ (i.e., small $r_0\kappa$), the double layer extends into the solution to distances comparable with the depletion layer, resulting in an increased or decreased transport limited current.

As $r_0\kappa \rightarrow 0$, the normalized limiting current asymptotically approaches limiting values for the reduction of A^+ and for the oxidation of A^- . The asymptotic limits are given in Table 1 and compared to the exact analytic solution (eq. 19) obtained using $\phi_0 = 0.1$ V and $z_j = -1$ and $+1$. The disparity between these two values is less than 1%, demonstrating the accuracy of the simulations.

Table 1. Normalized Mass-Transfer Currents as $r_0\kappa \rightarrow 0$.^a

| <u>Reaction</u> | <u>Analytical</u> . ^b | <u>Finite Difference Simulation</u> ^c |
|---------------------------|----------------------------------|--|
| $A^- \rightarrow A + e^-$ | 3.97 | 3.95 |



0.081

0.081

- a) The electrode potential is +0.1 vs E_{pzc}
 - b) eq. 19.
 - c) simulation conditions: $r_0 < 5 \text{ \AA}$; $C^b = 1 \text{ mM}$; no supporting electrolyte.
-

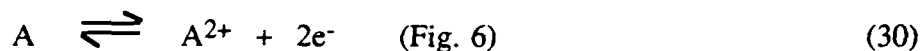
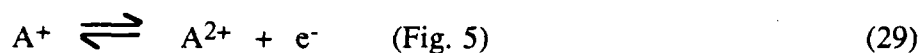
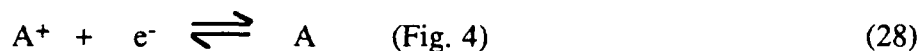
In the following section, we describe the overall steady-state voltammetric behavior of spherical microelectrodes in the limit $r_0\kappa \rightarrow 0$. Before describing the results, it is useful to consider the applicability of the analytic theory in predicting the behavior of real electrochemical systems. From Fig. 3, we find that normalized flux for the oxidation of A^- predicted by eq. 19 (which is exact in the limit $r_0\kappa \rightarrow 0$), is closely approximated by the simulated fluxes when $r_0\kappa < 0.1$. For the reduction of A^+ , the analytic and simulated values coincide when $r_0\kappa < 1.0$. Thus, the analytic solution (eq. 14) can be applied to approximate the behavior of these particular systems when $r_0\kappa$ is less than the abovementioned values. As a specific example, a 300 \AA radius electrode in an aqueous solution (25°C) containing $\sim 0.1 \text{ mM}$ of A^+X^- corresponds to $r_0\kappa = 1$. The voltammetric behavior of this system would, thus, be prescribed by eq. 14.

In general, the useful working range of eq. 14 is dictated by both the sign and magnitude of the dimensionless interaction energy, W_j (for both O and R), as well as $r_0\kappa$. Double layer effects on transport limited fluxes become more pronounced as W_j increases, which occurs when the species charge, z_j , or the electrode potential, ϕ_0 (E vs. E_{pzc}), is increased. In choosing to simulate the fluxes for the oxidation and reduction of a monovalent species (A^- or A^+) at low values of ϕ_0 (0.1V), we have, in effect, provided a very conservative estimate of the upper limit of $r_0\kappa$ for which eq. 14 is useful. At larger ϕ_0 , or when considering the oxidation or reduction of a multivalent species, the electrostatic forces influencing migrational currents will be more pronounced, causing the transition

between macroscopic behavior ($r_0\kappa \rightarrow \infty$) and microscopic behavior ($r_0\kappa \rightarrow 0$) to occur at larger values of $r_0\kappa$.

Voltammetry at Microelectrodes as $r_0\kappa \rightarrow 0$.

Eq. 14 was used to calculate the voltammetric behavior expected for following redox systems:



Each system exemplifies different types of behavior resulting from migration effects within the double layer. In each system, we have calculated the voltammograms assuming that both halves of the redox couple are soluble in solution, and that only the reactant (l.h.s. of eqs. 28, 29, and 30) is initially present in bulk solution. In plotting the voltammograms we have set E^0 equal to 0.0V vs. an unspecified reference electrode, allowing numerical values of E_{pzc} to be defined vs. E^0 . Numerical values of ϕ_0 correspond to $E - E_{pzc}$.

Fig. 4 shows the voltammetric response expected for the 1- e^- reduction of A^+ (eq. 28) for several values of E_{pzc} relative to E^0 and as a function of k_0D/r_0 . The sigmoidal shaped voltammograms (dashed curves) in Fig. 4 corresponds to classical diffusion-limited reduction ignoring double layer effects. When double layer effects are taken into consideration, the voltammetric current is increased or decreased depending on the relative values of E and E_{pzc} . For example, in Fig. 4a, when $E_{pzc} = 0$, the reduction of A^+ is enhanced greatly when the E is more negative than E_{pzc} , reflecting an attractive force between the negative electrode and positive ion. Conversely, when E is moved more

positive than E_{pzc} , electrostatic repulsion between the ion and electrode decreases the magnitude of the current. Voltammograms for $E_{pzc} = 0.1$ and $-0.1V$ vs. E^0 , also shown in Fig. 4a, can be qualitatively explained in a similar fashion. For reversible e^- - transfer, $k_{o,r}^0/D > 10^2$, the intercepts between the sigmoidal shaped diffusion-limited curve and the voltammograms including double layer effects occur at E_{pzc} in each case, corresponding to zero electrostatic force.

Fig. 5 shows voltammograms for the $1-e^-$ oxidation of A^+ to A^{2+} (eq. 29) for the same potential range and values of E_{pzc} as in Fig. 4. Here, the voltammograms have a skewed bell shape resulting from electrostatic repulsion of A^+ from the electrode at potentials that normally correspond to the diffusion limiting current plateau. At potentials sufficiently positive of E_{pzc} the limiting current is suppressed to negligible values. For instance, at an electrode where $E_{pzc} = 0$ vs E^0 , the limiting current at $E = 0.2V$ is reduced to 0.3% of the value in the absence of migration. For systems where E_{pzc} is more negative than E^0 , electrostatic repulsion effectively eliminates the voltammetric wave (Fig. 5).

Fig. 6 shows voltammograms for the $2e^-$ oxidation of A (eq. 30) for $(E_{pzc} - E^0) = 0.5$ and -0.5 V. In this case, reduction at sufficiently large overpotentials is controlled by diffusion of A to the surface resulting in a sigmoidal shaped curve with a well defined limiting current plateau. Near E^0 the migration of electrogenerated A^{2+} has a strong effect on the $E_{1/2}$ of the reaction. When $(E_{pzc} - E^0)$ is positive, migration of A^{2+} towards the electrode surface at potentials between E_{pzc} and E^0 increase the rate of back reaction resulting in a shift of $E_{1/2}$ to more positive potentials. For $(E_{pzc} - E^0) = 0.5$, $E_{1/2}$ is shifted ~ 0.25 V positive E^0 . When $(E_{pzc} - E^0) = -0.5$, migration of A^{2+} away from the surface decrease the rate of backreaction, shifting $E_{1/2}$ towards negative values. However, the effect is less in this case since migration of A^{2+} occurs only when the potential is sufficiently close to E^0 to cause the oxidation of A .

Also shown in Figs. 4, 5, and 6 is the effect of varying the dimensionless rate $k_0 r_0/D$ on the voltammetric waves. We plot curves for $k_0 r_0/D = 10^2$, 1, and 10^{-2} which in the limit of $W_j \rightarrow 0$ correspond to reversible, quasi-reversible, and irreversible electron-transfer reactions. For the reduction of A^+ (eq. 30), a decrease in $k_0 r_0/D$ has the effect of shifting the voltammetric curve to more negative values. At sufficiently negative values of the potential, mass-transfer becomes rate limiting and current is given by eq. 19. For the oxidation of A^+ (eq. 29), a decrease in $k_0 r_0/D$ shifts the foot of the wave to more positive potentials as expected. However, since migration of A^+ away from the surface at positive potentials effectively blocks the reaction, the bell-shaped voltammogram is diminished in size (note scale change between Fig. 5a and 5b). The effect of $k_0 r_0/D$ on the wave corresponding to oxidation of A (eq. 30) has a similar dependence on the position of E_{pzc} .

As a final note, because the potential decays slowly as r^{-1} away from an unscreened spherical electrode, (i.e., $\phi(r) = \phi_0(1 - r_0/r)$), only a fraction of the total applied potential (E vs E^0) that drives the electron-transfer reaction will be sensed by the reactant at the distance at which electron-transfer occurs, $r_{e.t.}$. In considering this effect, we assume that $r_{e.t.}$ is comparable or equal to the distance of closest approach of ions to the electrode surface without being specifically adsorbed (the outer Helmholtz plane, $\sim 2 - 10 \text{ \AA}$). We also assume that specific adsorption of the supporting electrolyte and dipole orientation at the surface make an insignificant contribution to the overall potential distribution. Under these conditions, the driving force for electron-transfer, $\eta_{corr.}$, at the distance $r_{e.t.}$ is given by eq. (31).

$$\eta_{corr.} = E(1 - r_0/r_{e.t.}) - E^0 \quad \text{eq. (31)}$$

Fig. 7 shows voltammograms for the $1-e^-$ oxidation and reduction of A^+ obtained by substituting $\eta_{corr.}$ (eq. 31) into eq. 14 and using values of $(1 - r_0/r_{e.t.}) = 0.02$ and 0.10

(corresponding approximately to 2 and 10 Å electron-transfer distances at a 100Å radius electrode). For comparison, we also show the case where $(1 - r_0/r_{e,t}) = 1$, corresponding to $\eta_{\text{corr.}} = \eta = E - E^{0'}$.

Conclusions. The simulations and theoretical analysis presented above yield the following conclusions regarding the steady-state current at submicron spherical electrodes:

- 1) A deviation from classical diffusion-migration limited currents is expected as the supporting electrolyte concentration or electrode radius is decreased. These deviations are the result of an increased effect of the electric field within the diffuse double layer. The numerical results provided in Fig. 3 provide an estimate of the ionic concentration and radius at which electrostatic double layer forces must be included in transport equations.
- 2) In the limiting case of $r_0\kappa \rightarrow 0$, the mass-transfer limited current to a spherical microelectrode, eq. 14, can be used to calculate the flux for multivalent species or electrode potential not considered here.
- 3) The voltammetric response of a spherical electrode as $r_0\kappa \rightarrow 0$ is non-classical in that a mass-transfer limiting current plateau is not expected for the reduction or oxidation of a charged reactant. The shape of the voltammogram depends on $E^{0'}$, E_{pzc} , r_0 , the supporting electrolyte concentration, as well as the reactant and product valencies. Figs. 4 and 5 show the magnitude of these effects for the reduction and oxidation of a +1 ion. The deviation of current-voltage from a sigmoidal shape will be more pronounced for multiply charge reactants.

4) The voltammetric response may be a function of the electrode work function since the E_{pzc} is a function of this parameter.

5) In drawing the analogy between bimolecular rate theory and voltammetry at submicron electrodes, we assumed that the reactant can be treated as a point charge (i.e. $r_{ion} = 0$). However, explicit inclusion of the reactant and product radii in the analysis indicates (see Appendix) that the magnitude and shape of the voltammetric curve will be weakly dependent on the size of the ionic reactant.

The results of this research have applications to several areas of electrochemistry. Many submicron systems exist in which the effect of the electric field within the diffuse double layer may affect electrochemical rates. For example, the fabrication and use of hemispherical mercury microelectrodes as small as $0.15 \mu\text{m}$ has been recently reported¹⁵. Several research groups are currently performing electrochemistry through the use of tips of scanning tunnelling microscopes^{16,17,18}. These tips typically range in diameter from 0.1 to $5 \mu\text{m}$ and can be characterized as hemispheres. Other applications include the electrochemical behavior of colloidal systems,^{19,20} and supported catalyst particles²¹.

Appendix.

Derivation of the Normalized Flux to a Spherical Microelectrode (eq. 19) from Diffusion Controlled Bimolecular Reaction Rate Theory. The rate, k_D , of a diffusion controlled bimolecular reaction between charged species was determined by Debye using Smoluchowski's method:

$$k_D = 4\pi N_A(D_A + D_B)(r_A + r_B) \frac{W}{e^W - 1} \quad (\text{A1})$$

$$W = \frac{z_A z_B e^2}{4\pi\epsilon\epsilon_0 kT(r_A + r_B)}$$

A and B represent the reacting ions with diffusivities D_A and D_B , and radii r_A and r_B , respectively. The factor $W/e^W - 1$ in eq. (A1) corresponds to the work required in bringing charged reactants together.

The steady-state flux of an ionic redox species to a charged spherical electrode can be obtained from eq. (A1) by letting B represent a stationary electrode ($D_B = 0$ and $r_B = r_0$) to which redox species A is diffusing. The effective "valency" of the electrode, z_A , is defined by eq. (1) of the text.

Combining eqs. (A1) and (20) and representing the redox species by point charges ($r_A = 0$) yields the expected current at a spherical electrode:

$$i_L = 4\pi n F C^b D_A r_0 \frac{W}{e^W - 1} \quad (\text{A2})$$

If either the electrode or reactant is uncharged, then:

$$i_L(\text{diff.}) = 4\pi n F C^b D_A r_0 \quad (\text{A3})$$

which is the diffusional current to a spherical electrode. Combining eqs. (A2) and (A3) yields the normalized current as $r_0 \kappa \rightarrow 0$:

$$\frac{i_L}{i_L(\text{diff.})} = \frac{W}{e^W - 1}$$

which is identical to eq. (19) in the text.

Acknowledgement. This work was supported by the Office of Naval Research Young Investigator Program.

Figure Captions

1. Diagram (*drawn to scale*) of the relative thicknesses of the diffuse double-layer and the diffusion layer, δ , ($\sim 10 r_0$) surrounding a 100\AA radius hemispherical electrode immersed in a 10^{-3} M aqueous solution of a 1:1 electrolyte. The spherically symmetric diffuse layer thickness is approximated as $2\kappa^{-1}$, corresponding to the distance from the surface where the electrical potential decays to $\sim 5\%$ of its surface value²².
2. Simulated diffuse double layer concentration profiles surrounding a spherical electrode in a 1:1 aqueous electrolyte. The surface potential (vs. E_{pzc}), electrolyte concentration, and electrode radius for each simulation are indicated in the figures.
3. Normalized steady-state flux as a function $r_0\kappa$ for various values of C_{redox}/C_{elec} . The diffusion limited current in the absence of migration, $i_L(diff.)$, is equal to $4\pi nFD C^b r_0$. The dashed lines ($i_L/i_L(diff.) = 3.975$ and 0.0809) correspond to eq. 19, the analytic value of the flux in the limit $r_0\kappa \rightarrow 0$. The dotted line ($i_L/i_L(diff.) = 2$) corresponds to the diffusion-migration limit (eq. 26) when the supporting electrolyte concentration is much smaller than the redox species concentration, $C_{redox}/C_{elec} \gg 1$.
4. Theoretical voltammograms calculated from eq. 14 for the reaction $A^+ + e^- \rightarrow A$ as a function of E_{pzc} , and $k_0 D/r_0$. The formal redox potential of the couple A^+/A , E^0' , is set equal to 0V vs. an arbitrary reference electrode. The dotted line indicates the diffusion limited reversible voltammograms.
5. Theoretical voltammograms calculated from eq. 19 for the reaction $A^+ \rightarrow A^{2+} + e^-$ as a function of E_{pzc} and $k_0 D/r_0$. The formal redox potential of the couple A^+/A , E^0' , is set

equal to 0V vs. an arbitrary reference electrode. The dotted line indicates the diffusion limited reversible voltammograms.

6. Theoretical voltammograms calculated from eq. 19 for the reaction $A \rightarrow A^{2+} + 2e^-$ as a function of E_{pzc} and k_0D/r_0 . The formal redox potential of A/A^{2+} , E^{01} , is set equal to 0V 05, an arbitrary reference electrode. The dotted line corresponds to the reversible diffusion limited voltammogram.

7. Theoretical voltammograms for the oxidation and reduction of A^+ showing the effect of the dimensionless electron-transfer distance, $(r_{e,t} - r_0)/r_0$, on the waveshape. Each curve corresponds to $k_0D/r_0 = X$, $E_{pzc} = E^{0'} = 0$, and

References

- 1 Adams, R. N., *Anal. Chem.*, **1976**, *48*, 1128A
- 2 Wightman, R. M., *Anal. Chem.* **1981**, *53*, 1125A
- 3 Morris, R. B., Franta, D. J., White, H. S., *J. Phys. Chem.*, **1987**, *91*, 3559.
- 4 Seibold, J. D., Scott, E. R., White, H. S. *J. Electroanal.*, **1989**, *264*, 281.
- 5 Shain, I.; Martin, K. J.; Ross, J. W. *J. Phys. Chem.* **1961**, *65*, 259.
- 6 Debye, P. *Trans. Electrochem. Soc.* **1942**, *82*, 265.
- 7 Smoluchowski, M. V. *Z. physik. Chem.* **1917**, *92*, 129.
- 8 Joslin, T.; Pletcher, D. J., *Electroanal. Chem.* **1974**, *49*, 171.
- 9 Feldberg, S. W., *J. Electroanal. Chem.* **1981**, *127*, 1.
- 10 Richtmyer, R. D.; Morton, K. W. *Difference Methods for Initial-Value Problems*, Interscience: NY, 1957.
- 11 Feldberg, S. W.; Norton, J. D. manuscript in preparation.
- 12 Loeb, A. L.; Overbeek, J. Th. G.; Wiersema, P. H. *The Electrical Double Layer Around a Spherical Colloid Particle*, MIT Press: Cambridge, 1960.
- 13 Heyrovsky, J. *Archiv Hem. Farm.* **1934**, *8*, 11.
- 14 ilkovic, D. *Collection Czechoslov. Chem. Commun.* **1934**, *6*, 498.
- 15 Pons, J. W.; Daschbach, J.; Pons, S.; Fleischmann, M. *J. Electroanal. Chem.* **1988**, *239*, 427.
- 16 Bard, A. J.; Fan, F.-R. F.; Kwak, J.; Ovadia, L.; *Anal. Chem.* **1989**, *61*, 132.
- 17 Penner, R. M.; Heben, M. J.; Lewis, N. S.; submitted for publication.
- 18 Scott, E. R.; White, H. S.; to be submitted.
- 19 Fleischmann, M.; Ghoroghchian, J.; Rolison, D.; Pons, S. *J. Phys. Chem.* **1986**, *90*, 6392.
- 20 Leland, J. K.; Bard, A. J. *J. Phys. Chem.* **1987**, *91*, 5076.
- 21 Sobczynski, A.; Bard, A. J.; Campion, A.; Fox, M. A.; Mallouk, T.; Webber, S. E.; White, J. M. *J. Phys. Chem.* **1987**, *91*, 3316.
- 22 The potential distribution around a sphere is given by $\phi(r)/\phi_0 = (r_0/r)\exp(-(r-r_0)\kappa)$ at low surface potential, ϕ_0 .

— 500Å —

